

# The intimate relation between the low T/W instability and the co-rotation point

A. Passamonti<sup>1\*</sup>, N. Andersson<sup>2</sup>

<sup>1</sup> *INAF-Osservatorio Astronomico di Roma, via Frascati 44, I-00040, Monteporzio Catone (Roma), Italy*

<sup>2</sup> *School of Mathematics and STAG Research Centre, University of Southampton, Southampton SO17 1BJ, UK*

3 September 2014

## ABSTRACT

We study the low T/W instability associated with the f-mode of differentially rotating stars. Our stellar models are described by a polytropic equation of state and the rotation profile is given by the standard j-constant law. The properties of the relevant oscillation modes, including the instability growth time, are determined from time evolutions of the linearised dynamical equations in Newtonian gravity. In order to analyse the instability we monitor also the canonical energy and angular momentum. Our results demonstrate that the  $l = m = 2$  f-mode becomes unstable as soon as a co-rotation point develops inside the star (i.e. whenever there is a point where the mode's pattern speed matches the bulk angular velocity). Considering various degrees of differential rotation, we show that the instability grows faster deep inside the co-rotation region and deduce an empirical relation that correlates the mode frequency and the star's parameters, which captures the main features of the  $l = m = 2$  f-mode growth time. This function is proportional to the product of the kinetic to gravitational energy ratio and the gradient of the star's spin, strengthening further the relationship between the co-rotation point and the low T/W instability. We briefly consider also the  $l = m = 2$  r-mode and demonstrate that it never moves far inside the co-rotation region even for significant differential rotation.

**Key words:** methods: numerical – stars: neutron – stars: oscillation – star:rotation.

## 1 INTRODUCTION

Rotating neutron stars may experience a host of non-axisymmetric instabilities, acting either on a dynamical or secular (e.g. associated with some dissipation mechanism) timescale. It is important to understand the range of possible instabilities, whether they are likely to act in a realistic astrophysical setting and possible repercussions on the evolution of the star. The most pressing issues have a direct connection with observations. In particular, because the unstable oscillation modes are non-axisymmetric they generate gravitational radiation and a number of plausible scenarios where this radiation may be detectable by advanced interferometers have been suggested. Presently, the most interesting scenarios involve dynamical instabilities triggered during the late stages of core-collapse or in the immediate aftermath of binary merger and gravitational-wave driven instabilities of more mature stars (associated with either the star's fundamental f-mode or the inertial r-mode). The main topic

of the present work, the so-called low T/W instability, is a relative late-comer to the discussion. Just like its classic cousins the dynamical bar-mode instability and the secular instabilities due to viscosity or gravitational radiation, this instability acts on the f-mode of the star. The main distinction is that the low T/W instability requires the star to be differentially rotating. The aim of this paper is to explore, in more detail than in previous work, the nature of this instability. In particular, we want to test the assertion that the instability becomes active as soon as the f-mode enters the co-rotation region (whenever there exists a point in the star where the mode appears stationary with respect to an inertial observer).

The study of instabilities of rotating stars has a long history. Work on Newtonian incompressible self-gravitating rotating ellipsoids, like the Maclaurin spheroids, provided the first instability criteria in terms of the parameter  $\beta = T/|W|$ , where  $T$  and  $W$  are, respectively, the kinetic and gravitational energy of the star (note that we will often omit the absolute values in referring to the low T/W instability in the text). Early work established that the dynamical bar-mode

\* E-mail: andrea.passamonti@oa-roma.inaf.it

instability sets in when a star reaches  $\beta_d = 0.27$  (Chandrasekhar 1969). For higher spins than this, a star can reach a new equilibrium configuration with lower energy, maintaining the same mass, volume and angular momentum. The instability is dynamical because it does not require any additional mechanisms, like internal viscosity or the coupling to radiation, to operate. Although the models that were considered early on were simplistic the results have been found to be robust. Recent relativistic numerical simulations of rotating stars with both polytropic and more realistic equation of state (EoS) have only adjusted this instability threshold slightly to  $\beta_d = 0.24\text{--}0.25$  (Shibata et al. 2000; Baiotti et al. 2007). However, this level of rotation cannot be achieved by a compressible star in uniform rotation, since the corresponding mass shedding limit is reached for  $\beta \simeq 0.1$ . To reach higher values of  $\beta$  the system must rotate differentially. However, it is still not clear that astrophysical systems will ever reach such large values of  $\beta$ , at least not for a sustained period (there is evidence of significant differential rotation being generated during core collapse but this phase is interrupted by the core bounce so any related instability do not have much time to grow).

The introduction of differential rotation brings new features to the problem. In particular, numerical simulations led to the discovery that stars with a higher degree of differential rotation can suffer dynamical instabilities even at much lower values,  $\beta \simeq 0.14$  (Centrella et al. 2001). The existence of this instability, now referred to as the low T/W instability, has been confirmed by a number of full 3D numerical simulations as well as in linear analyses. In some cases, the instability threshold has been shown to be as low as  $\beta \simeq 0.01$  (Shibata et al. 2002, 2003; Saijo et al. 2003). Despite these interesting results, we do not yet have a detailed understanding of the nature of this instability. It has been proposed that the instability originates from an energy transfer between the bulk motion and an oscillation mode (Watts et al. 2005), in a fashion that resembles the shear instability in thick accretion disks (the so-called Papaloizou-Pringle instability) (Papaloizou & Pringle 1984). One would expect this energy exchange to occur at the co-rotation point, where the pattern speed of a mode matches the local angular velocity of the star (see discussion later). In analogy with accretion disks it was suggested that the star's vortensity may indicate the resonant cavity where this instability can grow (Ou & Tohline 2006). However, for rotating stars this criterion does not seem completely satisfactory (at least this has not been demonstrated yet).

The low T/W instability has been studied in Newtonian and relativistic non-linear simulations, with different methods and distinct numerical codes. There is clear evidence that it may develop during stellar core-collapse (Ott et al. 2005, 2007; Scheidegger et al. 2008; Kuroda & Umeda 2010) and it has been seen in numerical evolutions of rapidly rotating cold neutron stars (Saijo & Yoshida 2006; Cerdá-Durán et al. 2007; Corvino et al. 2010). Recently, with the development of magneto-hydrodynamical simulations, the impact of the magnetic field on the dynamical instabilities has been explored (Camarda et al. 2009; Franci et al. 2013; Muhlberger et al. 2014). The results suggest that the bar-mode instability can be suppressed by a very strong magnetic field,  $B \gtrsim 10^{16}\text{G}$ . Analytical work, based on a rotating system with cylindrical geometry, has shown that the low T/W in-

stability can be similarly suppressed by a strong toroidal magnetic field  $B > 10^{16}\text{G}$  (Fu & Lai 2011). Numerical simulations that consider an initial poloidal seed magnetic field, which differential rotation subsequently winds up, have shown that the instability is not affected for poloidal fields  $B < 4 \times 10^{13}\text{G}$ . More interestingly, for  $B \geq 5 \times 10^{14}\text{G}$  a quadrupolar distortion may be amplified by magnetic effects (Muhlberger et al. 2014). Much more effort is required in order to explore the interplay between differential rotation, the star's magnetic field and various instabilities.

In this work we focus on the pure hydrodynamics problem; we ignore magnetic fields, the star's elastic crust, superfluid core etcetera. We study the low T/W instability by means of time-evolutions of the linearised Newtonian equations. We focus on stars with a polytropic EoS and assume that the differential rotation is given by the j-constant rotation law. The latter choice is motivated by simulations of both core-collapse and neutron star mergers that suggest that real systems stay rather close to this simple rotation law. Our main aim is to determine the instability growth time for varying degrees of differential rotation and connect the results with key features like the presence of a co-rotation point in the star. The analysis focuses on the  $l = m = 2$  f-mode (the bar-mode), which in general exhibits the strongest instability. We trace the instability as the degree of differential rotation is increased for a given star, monitoring key indicators like the canonical energy and angular momentum densities. This part of the analysis builds on the work of Saijo & Yoshida (2006), who considered the canonical angular momentum associated with the unstable mode for cylindrical stars, and showed that even though the canonical angular momentum grows due to the instability it remains zero at the co-rotation point. To speed up the numerical simulations and allow us to investigate a large parameter space we mainly use the Cowling approximation, i.e. we neglect the perturbation of the gravitational potential. This affects the mode-frequencies at the 20% level, which should not have significant influence on the qualitative behaviour that is our main focus.

## 2 THE PROBLEM

### 2.1 The Newtonian equations

As we are considering the problem of a differentially rotating star in Newtonian gravity, we need to solve the Euler equation, the continuity equation for mass conservation and the Poisson equation for the gravitational potential:

$$\left( \frac{\partial}{\partial t} + \mathbf{v} \cdot \nabla \right) \mathbf{v} = -\nabla (h + \Phi), \quad (1)$$

$$\frac{\partial \rho}{\partial t} = -\nabla \cdot (\rho \mathbf{v}), \quad (2)$$

$$\nabla^2 \Phi = 4\pi G \rho, \quad (3)$$

where  $G$  is the gravitational constant. In these equations, the scalar fields  $\rho$ ,  $h$  and  $\Phi$  represent, respectively, the mass density, the specific enthalpy and the gravitational potential, while  $\mathbf{v}$  is the fluid velocity.

To close the system of equations we need to provide an equation of state. In order to keep things simple, which

makes sense as we are mainly interested in qualitative features, we consider a polytropic model;

$$P = k\rho^\gamma, \quad (4)$$

where  $k$  is a constant and the adiabatic index is given by

$$\gamma \equiv \frac{d \log P}{d \log \rho} = 1 + \frac{1}{n}, \quad (5)$$

where  $n$  is the polytropic index.

For an axisymmetric equilibrium configuration, equations (1)-(3) can be written in integral form (Hachisu 1986),

$$h + \Phi + \Psi = C, \quad (6)$$

where  $C$  is an integration constant, and the gravitational potential is determined by the integral equation:

$$\Phi(\mathbf{r}) = -G \int_0^r \frac{\rho(\mathbf{r}')}{|\mathbf{r} - \mathbf{r}'|} d\mathbf{r}'. \quad (7)$$

In equation (6), the centrifugal potential  $\Psi$  is defined by:

$$\Psi = - \int \Omega^2 \varpi d\varpi, \quad (8)$$

where  $\Omega$  is the star's angular velocity and the cylindrical radius  $\varpi = r \sin \theta$  represents the distance of a fluid element from the rotation axis.

In a barotropic fluid, pressure and enthalpy are related by

$$h = \int \frac{dP}{\rho}, \quad (9)$$

which for a polytropic EoS leads to:

$$h = \frac{\gamma}{\gamma - 1} \frac{P}{\rho}. \quad (10)$$

## 2.2 Linear perturbations

In order to explore the unstable oscillations associated with the low  $T/W$  instability we need to solve the equations that govern linear perturbations of our differentially rotating configurations. Quite generally, non-axisymmetric small-amplitude oscillations of a differentially rotating star can be studied with a set of three scalar and one vector perturbation fields, namely the mass density  $\delta\rho$ , the enthalpy  $\delta h$ , the gravitational potential  $\delta\Phi$  and the velocity perturbation  $\delta\mathbf{v}$ . These variables satisfy a system of linearised equations which, for an inertial observer and in spherical coordinates  $[r, \theta, \phi]$ , reads

$$\left( \frac{\partial}{\partial t} + \Omega \frac{\partial}{\partial \phi} \right) \delta\mathbf{v} = -\nabla(\delta h + \delta\Phi) - 2\boldsymbol{\Omega} \times \delta\mathbf{v} - (\delta\mathbf{v} \cdot \nabla\Omega) r \sin\theta \hat{e}_\phi, \quad (11)$$

$$\left( \frac{\partial}{\partial t} + \Omega \frac{\partial}{\partial \phi} \right) \delta h = -\frac{\partial \rho}{\partial h} \nabla \cdot (\rho \delta\mathbf{v}), \quad (12)$$

$$\nabla^2 \delta\Phi = 4\pi G \delta\rho. \quad (13)$$

In equation (11) we have used the  $\phi$ -component of the orthonormal basis vectors;  $\hat{e}_\phi$ .

To simplify the numerical study of equations (11)-(13) we perform a Fourier expansion of the variables with respect to the  $\phi$ -angle, leading to the introduction of the azimuthal harmonic index  $m$ . This way, we only have to solve a two-dimensional problem in space, rather than the original

three-dimensional one (Papaloizou & Pringle 1980). For any perturbation variable we use an expansion, analogous to the following for the mass density;

$$\delta\rho(t, r, \theta, \phi) = \sum_{m=0}^{m=\infty} [\delta\rho_m^+(t, r, \theta) \cos m\phi + \delta\rho_m^-(t, r, \theta) \sin m\phi]. \quad (14)$$

For any  $m$ , we numerically evolve a system of ten partial differential equations for the twelve variables  $(\delta\mathbf{v}^\pm, \delta h^\pm, \delta\Phi^\pm, \delta\rho^\pm)$ , while the density perturbation is determined from the EoS. For our polytropic stars,  $\delta\rho$  is simply given by

$$\delta\rho = \frac{\rho}{c_s^2} \delta h, \quad (15)$$

where the speed of sound is defined by

$$c_s^2 = \frac{\partial P}{\partial \rho} = k\gamma\rho^{\gamma-1}. \quad (16)$$

Finally, we introduce the Lagrangian displacement vector  $\boldsymbol{\xi}$ . This is a key quantity in the instability criteria developed by Friedman & Schutz (1978a), and we also need it to implement some of the boundary conditions associated with the problem. We determine the Lagrangian displacement by evaluating (Friedman & Schutz 1978a):

$$\delta\mathbf{v} = \frac{\partial \boldsymbol{\xi}}{\partial t} + \mathbf{v} \cdot \nabla \boldsymbol{\xi} - \boldsymbol{\xi} \cdot \nabla \mathbf{v}, \quad (17)$$

at each time step during the numerical simulations.

## 2.3 Boundary conditions

The evolution equations need to be complemented by boundary conditions. At the stellar surface we require that the Lagrangian perturbation of the enthalpy vanishes, i.e.,

$$\Delta h = \delta h + \boldsymbol{\xi} \cdot \nabla h = 0. \quad (18)$$

We satisfy this boundary condition by imposing the condition

$$\delta h = -\boldsymbol{\xi} \cdot \nabla h, \quad (19)$$

at the surface. All other variables are extrapolated at the surface grid point at each time step and the gravitational potential is determined by solving the Poisson equation.

For non-axisymmetric oscillations with  $m \geq 2$ , the regular behaviour of equations (11)-(13) at the origin,  $r = 0$ , and on the rotational axis,  $\theta = 0$ , is guaranteed by the conditions:

$$\delta h = \delta\rho = 0, \quad \text{and} \quad \delta\mathbf{v} = \mathbf{0}. \quad (20)$$

Finally, at the equator,  $\theta = \pi/2$ , the perturbation variables divide in two classes with opposite reflection symmetry. In the first class, the variables  $\delta\rho^+$ ,  $\delta\Phi^+$ ,  $\delta v_r^+$ ,  $\delta v_\phi^+$  are all even under reflection with respect to the equatorial plane, while  $\delta v_\theta^-$  is odd. By contrast, for the second class  $\delta\rho^-$ ,  $\delta\Phi^-$ ,  $\delta v_r^-$ ,  $\delta v_\phi^-$  are odd and  $\delta v_\theta^+$  is even.

## 2.4 Differentially rotating models

We construct models of rapidly and differentially rotating polytropes by solving equations (6)-(8) for a given rotation law. Following much of the relevant literature on the subject,

**Table 1.** This table lists key quantities for three sequences of differentially rotating equilibrium configurations. The stellar models are described by a  $\gamma = 2$  polytropic equation of state and the j-constant rotation law. The first column gives the parameter  $A$  that controls the degree of differential rotation. In the second and third columns, we provide, respectively, the ratio of polar to equatorial axes and the parameter  $j_0$ . The mass, maximum pressure, angular momentum and the rotational parameter  $\beta = T/|W|$  are given in the last four columns, respectively. All quantities are expressed in dimensionless units, where  $G$  is the gravitational constant,  $\rho_m$  represents the maximum mass density and  $R_{eq}$  is the equatorial radius.

$A/R_{eq}$	$R_p/R_{eq}$	$j_0/(\sqrt{G\rho_m}R_{eq}^2)$	$M/(\rho_m R_{eq}^3)$	$p_m/(GR_{eq}^2\rho_m^2)$	$J/(G^{1/2}\rho_m^{3/2}R_{eq}^5)$	$\beta \times 10^2$
1.0	1.0	0.000	1.273	0.637	0.000	0.00
1.0	0.9	0.569	1.167	0.570	0.125	2.49
1.0	0.7	0.964	0.947	0.431	0.174	8.36
1.0	0.5	1.189	0.718	0.285	0.165	15.82
1.0	0.3	1.337	0.558	0.149	0.152	25.57
0.5	0.9	0.231	1.229	0.585	0.125	2.33
0.5	0.7	0.413	1.161	0.474	0.219	7.72
0.5	0.5	0.547	1.116	0.359	0.294	14.07
0.5	0.3	0.605	0.997	0.259	0.318	20.05
0.5	0.1	0.593	0.891	0.209	0.299	22.43
0.1	0.9	0.049	1.329	0.623	0.059	0.80
0.1	0.7	0.091	1.356	0.592	0.114	2.53
0.1	0.5	0.121	1.355	0.559	0.152	4.23
0.1	0.3	0.143	1.344	0.531	0.531	5.59
0.1	0.1	0.154	1.336	0.515	0.193	6.36

we assume the so-called j-constant rotation law, which is defined by

$$\Omega = \frac{j_0}{A^2 + r^2 \sin^2 \theta}, \quad (21)$$

where  $j_0$  is a constant and  $A$  is a parameter that controls the degree of differential rotation. In the limit of small  $A$ , equation (21) generates a configuration with constant specific angular momentum (hence the name of the rotation law), while for large  $A$  the star tends to uniform rotation. The constant  $j_0$  can be easily obtained by considering equations (21) on the rotation axis, which leads to  $j_0 = \Omega_c A^2$ , where  $\Omega_c$  is the star's angular velocity on the rotation axis.

In practice, we solve equations (6)-(8) by means of the self-consistent field method described by Hachisu (1986). This consists of an iterative numerical procedure, which can be started by giving as an input the polytropic index of the EoS, the ratio of the polar to equatorial axes  $R_p/R_{eq}$ , and the degree of differential rotation via the parameter  $A$ . Our numerical code for determining differentially rotating stars builds on the code developed by Jones et al. (2002) to study uniformly rotating configurations.

In Table 1 we provide data for three sequences of differentially rotating models. The models are described in terms of dimensionless quantities obtained from the maximum density  $\rho_m$ , equatorial radius  $R_{eq}$  and gravitational constant  $G$  (as in for instance Hachisu 1986). Note that, in dimensionless units the differential rotation parameter is given by  $\hat{A} = A/R_{eq}$ . Nevertheless, we will for clarity use  $A$  instead of  $\hat{A}$  in the discussion of the results.

From the data reported in Table 1, we can construct different sequences of rotating stars, eg. with constant mass or constant angular momentum. For instance, by specifying the mass of the star  $M$  and the EoS parameters  $k$  and  $\gamma$ , we can obtain the equatorial radius and the maximum mass

density in physical units from the following expressions:

$$R_{eq} = \left[ \frac{1}{G} \frac{k}{\hat{k}} \left( \frac{M}{\hat{M}} \right)^{\gamma-2} \right]^{1/(3\gamma-4)}, \quad (22)$$

$$\rho_m = M \hat{M}^{-1} R_{eq}^{-3}, \quad (23)$$

where for a polytropic EoS  $\hat{k}$  is equal to the maximum dimensionless pressure  $\hat{p}_m$ , and the “hats” denote the dimensionless quantities listed in Table 1.

## 2.5 Code description and tests

Having determined suitable background configurations, we set up a numerical code that evolves in time the system of hyperbolic perturbation equations (11)-(12), and at the same time solves (at each time step) the perturbed Poisson equation (13). The part of the code that evolves the hyperbolic equations uses the technology that was developed in previous work (Passamonti et al. 2009a,b), whereas the elliptic equation (13) is solved by means of a spectral method. The numerical grid is bidimensional and covers the volume of star in the region  $0 \leq r \leq R(\theta)$  and  $0 \leq \theta < \pi/2$ . With the definition of a new radial coordinate  $x = r/R(\theta)$ , we can associate each grid point with a fluid element of the star, even when the star is highly deformed by rotation. The perturbation variables that obey the hyperbolic differential equations (11)-(12) are discretized on the grid and updated in time with a Mac-Cormack algorithm. Finally, the numerical simulations are stabilised from high frequency noise with the implementation of a fourth order Kreiss-Oliger numerical dissipation  $\varepsilon_D D_4 \xi$ , with  $\varepsilon_D \approx 0.01$ . More technical details on the numerical implementation can be found in Passamonti et al. (2009a,b).

Most of the results presented in this paper were obtained using a  $48 \times 90$  grid to cover the  $\theta$  and  $r$  coordinates,

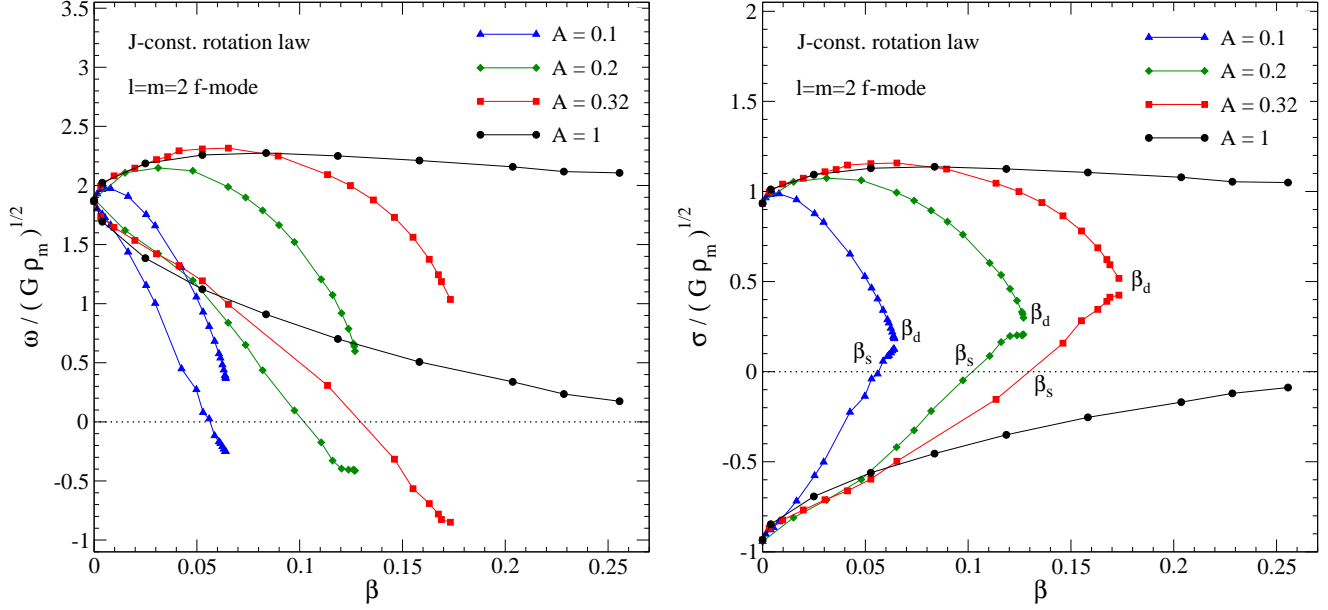


**Figure 1.** This figure shows the  $l = m = 2$  f-mode frequency (left-hand panel) and the pattern speed (right-hand panel) with respect to the star’s rotation  $\beta = T/|W|$  for four sequences of differentially rotating stars with, respectively,  $A = 0.1, 0.2, 0.32$  and 1. The mode frequency and pattern speed are given in dimensionless units. The horizontal dotted line in each panel denotes the neutral line of the secular instability,  $\beta_s$ , where an initially retrograde mode (according to an inertial observer) becomes prograde as a result of star’s rotation. The critical value  $\beta_d$  (indicated in the right panel) denotes the points in the  $\beta - \sigma$  plane where the two branches of  $l = m = 2$  f-mode merge and, consequently, the dynamical bar-mode instability is expected to develop.

respectively. In order to test the accuracy of our growth time extraction we evolved some models with a  $96 \times 180$  grid. This showed that the numerical error in the key quantities was significantly less than 1%, which means that the conclusions we draw from the results should be reliable.

### 3 THE LOW $T/W$ INSTABILITY

Our main interest is to trace the onset of the low  $T/W$  instability along a given sequence of differentially rotating stars. Specifically, we want to test the assertion of Watts et al. (2005) that the instability is present as soon as the f-mode enters the co-rotation region, i.e. whenever there is a point in the star (the co-rotation point) where the pattern speed of the mode matches the local rotation velocity. That is, when we have

$$\sigma = \Omega(\varpi_c), \quad (24)$$

where  $\sigma = \omega/m$  is the pattern speed of the mode and  $\varpi_c$  is the co-rotation point. Following the logic of the analogous instability in accretion disks (Papaloizou & Pringle 1984) one would expect this situation to allow for an exchange of energy between the mode and the bulk flow, thus causing the instability. Previous work has not had the “precision” to consider this issue in detail. Basically, while full 3D nonlinear simulations have demonstrated that the f-mode has to be well inside the co-rotation region for the instability to be active, they have not resolved the problem near the edge of the co-rotation region. Our perturbative framework is better suited for such an analysis. Of course, we will not be able to make any statements about the nonlinear saturation of

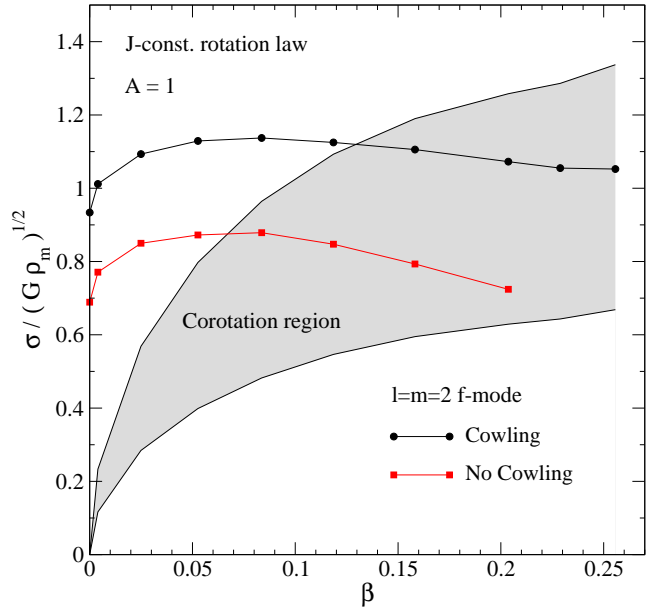


**Figure 2.** The pattern speed,  $\sigma = \omega/m$ , of the  $l = m = 2$  f-mode is shown as a function of the rotation parameter  $\beta$  for differentially rotating stars with  $A = 1$ . The black (dots) and red (squares) show the values of  $\sigma$  from our simulations, respectively, in the Cowling and non-Cowling approximation case. The co-rotation band is represented by the grey region.

the instability or the backreaction on the star, for which a nonlinear analysis is essential.

Seminal work on non-axisymmetric instabilities in ro-

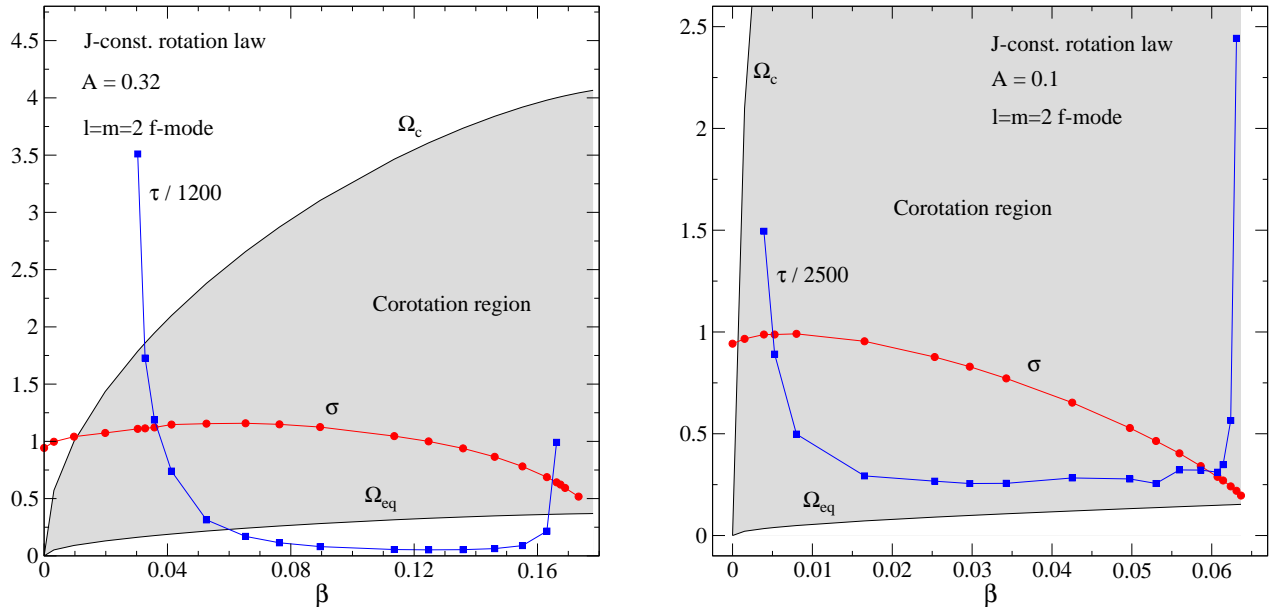


**Figure 3.** This figure provides the inferred shear instability growth time,  $\tau$ , for differentially rotating stars with  $A = 0.32$  (left-hand panel) and  $A = 0.1$  (right-hand panel). We also show the f-mode pattern speed,  $\sigma$ , and the co-rotation region (grey).

tating bodies (Friedman & Schutz 1975, 1978a,b) identified key quantities which can be used to monitor the development of an instability; the canonical energy and angular momentum. In an inviscid system a dynamical instability can develop only if these canonical quantities both vanish. This guarantees that an unstable mode does not violate the energy and angular momentum conservation laws. At first, one might think that it ought to be straightforward to use our results to confirm this expectation. Unfortunately, this is not the case. First of all, it is not clear that our extraction of the eigenfunctions, which are required for the evaluation of the canonical quantities, is accurate enough due to the growth of the perturbation variables during the evolution. Not only are the eigenfunctions contaminated by numerical noise, there may also be traces of other oscillation modes that are present during the evolution. Secondly, the instability criterion strictly holds only for inviscid systems. In our case, it is not clear what effect the numerical viscosity has on the analysis. In principle, one could argue that a numerical simulation provides the “exact” (inviscid) result as long as the code is convergent. One may, for example, try to extrapolate towards infinite resolution from a set of results with different numerical resolution. Unfortunately, our method is not good enough for us to be able to test this strategy. The same is true for the Jordan chain argument from (Schutz 1980a,b), which indicates the degeneracy associated with the merger of two linear perturbation modes (as for example in the case of the classic bar-mode instability at  $\beta_d$ , see Fig. 1).

Nevertheless, the canonical energy and angular momentum provide important measures. In terms of the enthalpy,

the canonical energy is given by (Friedman & Schutz 1978a):

$$E_c = \frac{1}{2} \int d\mathbf{r} \left[ \rho |\partial_t \xi_i|^2 - \rho |v^j \nabla_j \xi_i|^2 + \rho \xi^i \xi^{j*} \nabla_i \nabla_j (h + \Phi) + \frac{\partial h}{\partial \rho} |\delta \rho|^2 - \frac{1}{4\pi G} |\nabla_i \delta \Phi|^2 \right], \quad (25)$$

while the canonical angular momentum follows from (Friedman & Schutz 1978a):

$$J_c = -Re \int d\mathbf{r} \rho \partial_\phi \xi^{i*} \left( \partial_t \xi_i + v^j \nabla_j \xi_i \right), \quad (26)$$

where the integrals are calculated over the star’s volume, and  $Re$  denotes the real part. Note that these expressions are given in a coordinate basis, not the orthonormal basis used elsewhere in the paper. Building on the work of Saijo & Yoshida (2006) we will use the integrands from equations (25) and (26) to identify the region in the star where the instability develops.

### 3.1 The f-mode

As we have already mentioned, the current understanding is that the low T/W instability sets in when the f-mode enters the co-rotation region. In order to support this notion, it is natural to determine the mode frequencies along a differential rotation sequence and at the same time keep track of the co-rotation region. The latter task is straightforward since it only requires the background configurations. The determination of the oscillation frequencies for a set of stars along a given sequence is more time consuming. We obtain the required results by first evolving in time the linearised dynamical equations (11)–(13), and then calculating the mode frequencies by performing a Fast Fourier Transformation (FFT) on the time evolution data. In order to test the reliability of the method we have confirmed that the

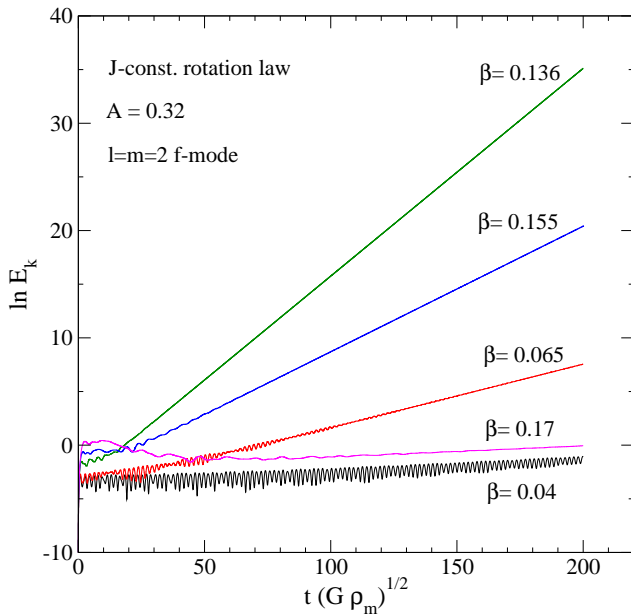


**Figure 4.** A sample of results for the time evolution of the kinetic energy associated with the  $f$ -mode for models with  $A = 0.32$  and different values for the rotation parameter  $\beta$  (see legend). The evolution time and the kinetic energy are given in dimensionless units. The vertical axis displays the natural logarithm of the kinetic energy,  $\ln E_k$ .

results agree with data available in the literature (Karino et al. 2001; Karino 2003).

Fig. 1 shows the  $l = m = 2$   $f$ -mode frequencies, measured in the inertial reference frame, for four sequences of models with a different degree of differential rotation. The stars with the lowest level of differential rotation are parameterised by  $A = 1$ , while the highest differential rotation models have  $A = 0.1$ . For small values of  $A$  the fastest spinning stellar models assume a “toroidal-like configuration” with a small axis ratio and a mass density whose maximum is not at the rotation axis. For instance, for  $A = 0.1$  the fastest model studied in this work has  $\beta = 0.064$  and  $R_p/R_{eq} = 0.067$ .

As expected, the results show that the  $f$ -mode is rotationally split into two branches which are, respectively, prograde and retrograde with respect to the star’s rotation. The prograde  $f$ -mode frequency gradually decreases for higher differential and more rapidly rotating models. Meanwhile, the retrograde  $f$ -mode has an oscillation frequency which decreases with rotation and can become negative for rapidly rotating models. The neutral point, where the  $f$ -mode frequency is zero (indicated by  $\beta_s$  in Fig. 1), is important as it marks the point where an  $f$ -mode is driven unstable by gravitational radiation via the well-known Chandrasekhar-Friedman-Schutz (CFS) mechanism (Chandrasekhar 1970; Friedman & Schutz 1975, 1978a). This secular instability occurs when a locally retrograde mode is dragged forward by the star’s rotation to the point where it is seen to be prograde by an inertial observer.

The conditions for the classical non-axisymmetric instabilities are better illustrated in the right-hand panel of Fig. 1, which shows the pattern speed,  $\sigma$ , for the  $l = m = 2$   $f$ -mode against the rotation parameter  $\beta$ . The results in the figure can be compared to the results for incompressible el-

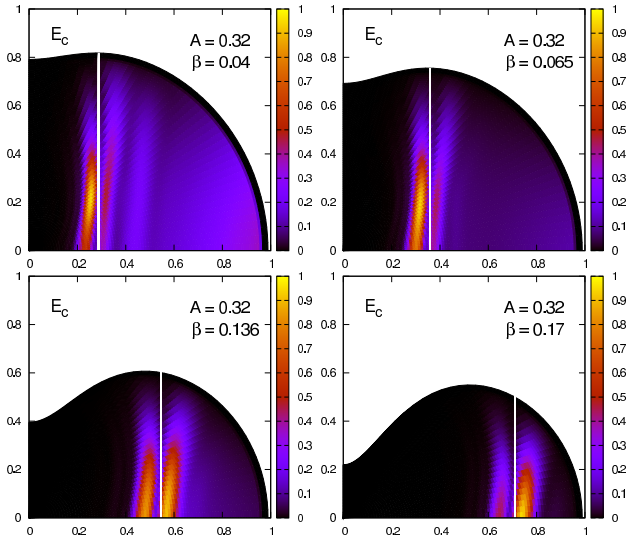


**Figure 5.** Examples of the extracted canonical energy density inside the neutron star. The vertical white line in each panel denotes the co-rotation cylindrical radius  $r_{cor}$ .

lipsoids (cf. Fig. 5 in Andersson 2003). When a mode has a negative (positive) pattern speed, it is retrograde (prograde) with respect to the star. For the models shown in Fig. 1 with  $A \leq 0.32$ , it is clear that the  $f$ -mode is retrograde for slowly rotating stars, but becomes prograde at the critical rotation rate corresponding to  $\beta_s$ . Another significant point in the  $\beta - \sigma$  parameter space is where the pattern speeds of the two branches of the  $f$ -mode merge. This point indicates where the modes merge and the classic dynamical bar-mode instability sets in in an inviscid star. Using our perturbative time evolutions we are able to extract the mode frequencies very close to this point,  $\beta_d$ , for the  $A = 0.1, 0.2$  and  $0.32$  sequences.

The part of the parameter space where the low  $T/W$  instability might occur is shown in Fig. 2 for stellar models with  $A = 1$  and in Fig. 3 for  $A = 0.32$  and  $0.1$ . For high differential rotation (small  $A$ ), the co-rotation region increases considerably and the  $l = m = 2$   $f$ -mode can enter this potential instability zone even for very slowly rotating stars. In Fig. 2, we also show the  $f$ -mode frequency calculated with the full perturbation problem, i.e. when the Poisson equation for the gravitational potential is solved alongside the fluid equations. It is well known that the Cowling approximation (where the gravitational potential perturbation is neglected) may introduce a significant error in the  $f$ -mode frequency (Karino 2003). As we can see from Fig. 2, the  $f$ -mode frequencies are generally smaller when  $\delta\Phi$  is included. In the present context this is important since it affects the relation between the mode-frequency and the co-rotation band. As indicated in the Figure, the inclusion of the gravitational potential means that the instability may be triggered at lower rotation rates. Unfortunately, the solution of the Poisson equation (an elliptic equation), slows down the numerical simulations significantly which increases the time it would take to perform a large parameter space analysis. In addition, for differentially rotating models our code is more stable when the Cowling approximation is used. Since we do not expect the Cowling approximation to have any effect on



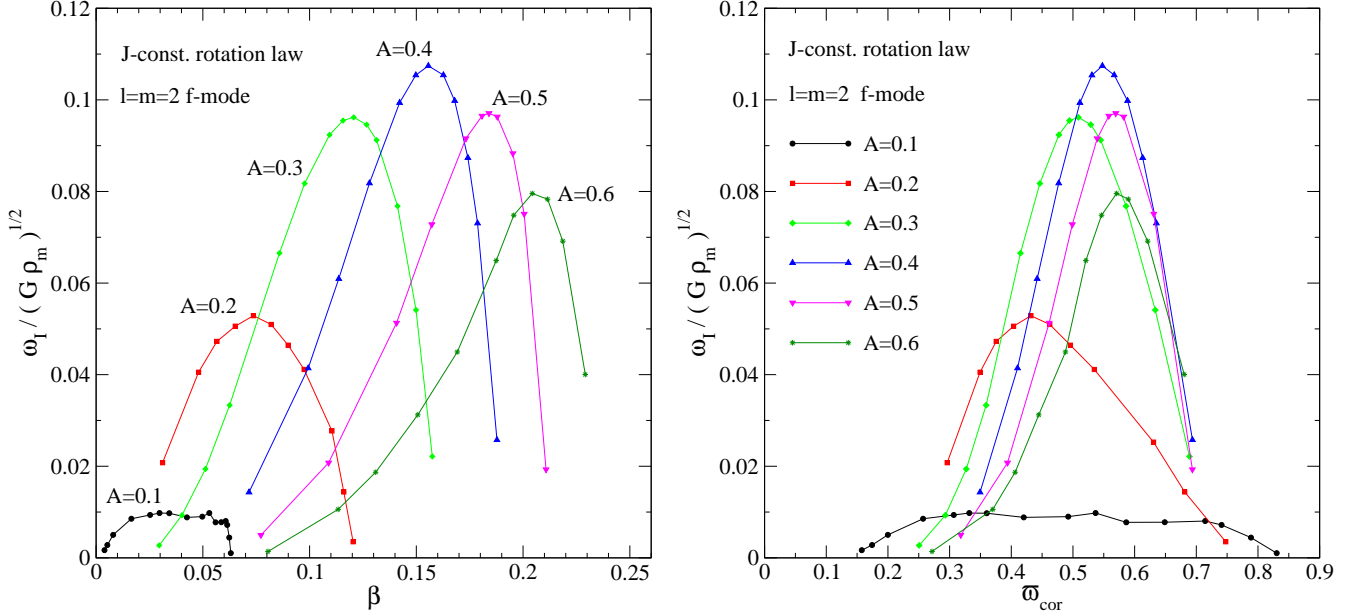


**Figure 6.** Imaginary part of the  $l = m = 2$  mode frequency,  $\omega_I = 2\pi/\tau$ , for several sequences of differentially rotating stars with  $A = 0.1 - 0.6$ . The left- and right-hand panels show the dependence of  $\omega_I$ , respectively, on the rotational parameter  $\beta$  and the cylindrical co-rotation radius  $\varpi_{cor}$ . The quantities on the horizontal and vertical axes are given in dimensionless units.

the qualitative behaviour of the low T/W instability we will from now on focus on results obtained by neglecting  $\delta\Phi$ .

### 3.2 Instability growth time

If the hypothesis from Watts et al. (2005) is correct, then the growth rate of the instability should depend on the position of the mode relative to the boundary of the co-rotation region, being more rapid deep inside the co-rotation region and essentially vanish at the co-rotation boundaries (as the mode stabilizes).

In order to assess this idea we determine the instability growth timescale from our numerical simulations. As an example, we show in Fig. 4 the mode kinetic energy,  $E_k$ , for the rotating star models with  $A = 0.32$ . After some evolution time, the kinetic energy starts to grow exponentially with a rate that depends on the stellar rotation. We determine the instability growth time,  $\tau$ , from a linear fit to the time evolved kinetic energy by assuming that

$$E_k \sim e^{2\omega_I t}, \quad \text{where } \omega_I = \frac{2\pi}{\tau}. \quad (27)$$

The kinetic energy is defined by the following equation:

$$E_k = \frac{1}{2} \int dr \rho \delta v^2. \quad (28)$$

For this specific model, we find that the instability timescale initially decreases as the rotation increases from a model with  $\beta = 0.04$  up to a model with  $\beta = 0.136$ , and then increases again for more rapidly rotating configurations, i.e.  $\beta = 0.17$ . The rescaled growth times for the  $A = 0.32$  and  $0.1$  cases are shown in Fig. 3, together with the pattern speed and the co-rotation region. The results clearly show that that  $\tau$  increases towards the boundaries of the co-rotation region. In fact, for models very close to these boundaries our time evolutions do not exhibit any instability. Most likely

this is due to the numerical viscosity in the code preventing the instability from setting in until the physical growth overcomes the artificial damping. Real viscosity would, of course, play a similar role but it is orders of magnitude weaker than the numerical viscosity used in our simulations.

In order to test the effect of the artificial viscosity on the inferred instability growth time we have considered several simulations with different numerical dissipation strength for a given stellar configuration. Thus we found that  $\tau$  is affected by the Kreiss-Oliger dissipation only at the level of about 0.1% even when the viscosity factor is an order of magnitude larger than the fiducial one used,  $\epsilon_D = 0.01$ . Hence, the extracted growth times are not significantly affected by the artificial damping. Of course, it is still the case that the numerical damping will overcome the growth of a very slowly growing unstable mode, e.g. near the co-rotation boundary.

In order to check that we are tracking a given unstable mode along the stellar sequence, we monitor the canonical energy and angular momentum integrands (see equations 25-26). Qualitatively, one would expect the unstable mode to be associated with the region near the co-rotation point in the star. If the low T/W instability is the result of an energy exchange between a co-rotating mode and the fluid bulk flow, this should be reflected in the energy and angular momentum integrands. This behaviour was, in fact, observed for the canonical angular momentum by Saijo & Yoshida (2006), who showed that the  $J_c$  integrand grows when an instability is present while remaining zero at the co-rotation point.

To study the behaviour of  $E_c$  and  $J_c$  it is useful to determine the cylindrical radius,  $\varpi_{cor}$ , at which a given mode co-rotates with the star (where  $\varpi = r \sin \theta$ ). For the j-constant rotation law, we can determine from equation (21) and the mode frequency,  $\omega$ , the following expression for the



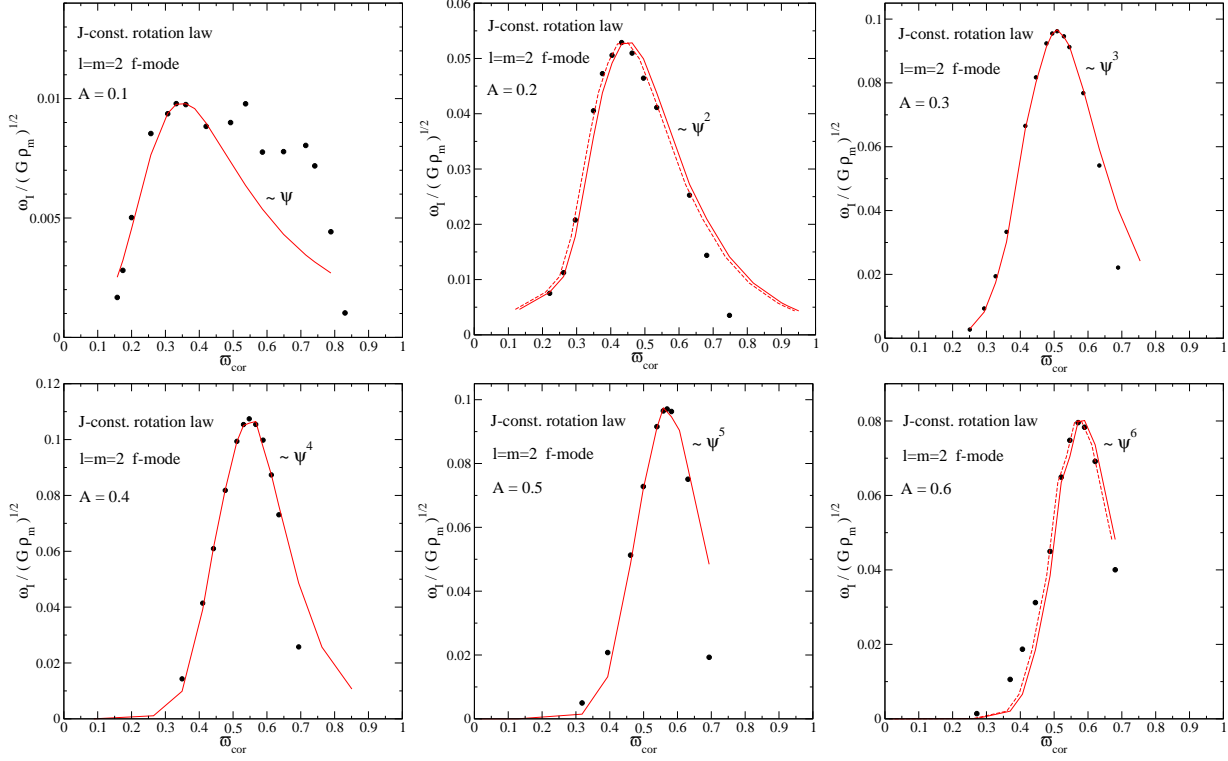


**Figure 7.** Comparison between the imaginary part of the  $l = m = 2$  f-mode and the empirical function  $\chi$  for six differentially rotating models. Each panel corresponds to a model with a specific  $A$  (see legend). The horizontal and vertical axes show, respectively, the dimensionless  $\varpi_{cor}$  and  $\omega_I$ . The filled dots represent the numerical values and the red lines the function  $\chi$ . In the panels for the  $A = 0.2$  and  $0.6$  models we also show a dashed red line, which provides a correction of the function  $\chi$  to match the  $\omega_I$  values.

co-rotation point:

$$\varpi_{cor} = A \sqrt{\frac{m\Omega_c - \text{Re } \omega}{\text{Re } \omega}}. \quad (29)$$

In Fig. 5 we show the canonical energy distribution inside the star and the co-rotation radius  $\varpi_{cor}$  calculated from equation (29), for a selection of unstable models with  $A = 0.32$ . As expected,  $E_c$  grows around the co-rotation point and vanishes at  $\varpi_{cor}$ . The same feature has been observed for the canonical angular momentum. These results confirm that the growth time extracted from our numerical simulations is associated with the  $l = m = 2$  f-mode (as expected).

The dependence of the instability growth time on the position of the co-rotation point is evident from Fig. 2. In order to understand the behaviour better, we consider the variation of  $\tau$  with the degree of differential rotation and try to relate the results with the stellar parameters. Typical results are provided in Fig. 6, where we show the variation of the unstable mode's imaginary part,  $\omega_I = 2\pi/\tau$ , with respect to the rotation parameter  $\beta$  (left-hand panel) and cylindrical co-rotation radius (right-hand panel) for stars with  $A$  ranging between 0.1 and 0.6. Note that  $\varpi_{cor} = 0$  corresponds to the condition  $\sigma = \Omega_c$ , while  $\varpi_{cor} = 1$  implies that  $\sigma = \Omega_{eq}$ . Along each rotating sequence, corresponding to a specific  $A$ ,  $\omega_I$  exhibits a maximum inside the co-rotation band and decays towards the boundaries of the region. It is also interesting to note that for higher differential rotation the instability region appears at smaller rotation rates.

The results in Fig. 6 make qualitative sense given our expectations for the low  $T/W$  instability, but we would obviously like to understand the detailed features better. There are two main aspects to this. First of all, the maximum  $\omega_I$  is not centred in the middle of the co-rotation band, where  $\varpi_{cor} = 0.5$ . Secondly,  $\omega_I$  appears to reach its largest absolute value in the  $A = 0.4$  model.

If the shear instability depends on an energy exchange between the bulk motion and the co-rotating mode, one would expect the instability timescale to depend on the energy and degree of differential rotation present at the co-rotation point. Considering the behaviour of the variables involved, we find that the function;

$$\psi = -\beta \left. \frac{\partial \Omega}{\partial \varpi} \right|_{\varpi_{cor}}, \quad (30)$$

where the derivative of the star's angular velocity is calculated at the co-rotation radius, has a maximum at the same point as  $\omega_I$  along the stellar sequence. Actually, we find that  $\psi$  increases from  $A = 0.1$  to  $0.5$  and then decreases. Hence, the function  $\psi$  accounts reasonably well for the main features observed in our results, eg. the faster instability growth of the model with  $A \sim 0.4$ . Moreover, for each rotating model (with a given  $A$ ) the function  $\psi$  can be used to determine the position of the shortest growth time inside the instability region.

It is worth noting that  $\psi$  can be re-written in terms of the star's parameters and the mode's pattern speed, using

**Table 2.** The dimensionless values of the coefficient  $a$ , see equation (32), for stellar models with  $A = 0.1 - 0.6$ .

$A$	0.1	0.2	0.3	0.4	0.5	0.6
$a$	0.072	0.74	2.32	5.26	12.4	32.9

equation (29),

$$\psi = \frac{2\beta}{A\Omega_c} (\Omega_c - \sigma)^{\frac{1}{2}} \sigma^{\frac{3}{2}}. \quad (31)$$

Our numerical data suggest that  $\omega_I$  is reasonably well approximated by the following empirical relation;

$$\chi = a \psi^{10A}, \quad (32)$$

where  $a$  is a constant, and  $A$  is the usual differential rotation parameter. For the various models considered in this work the function  $\chi$  is shown in Fig. 7, while the corresponding (dimensionless) values of  $a$  are given in Table 2. The maximum and the behaviour at small co-rotation radii are well captured by  $\chi$ , there is a slight horizontal offset for  $A = 0.2$  and  $0.6$  but they only amount to 1-2 % with respect to the  $\omega_I$  peak. For larger  $\varpi_{cor}$ , the function  $\chi$  generally assumes slightly larger values than  $\omega_I$ , while for  $A = 0.1$  the opposite is the case. For the latter model, this behaviour could be due to the presence of other unstable modes, but we did not manage to resolve this issue with our simulations.

Considering the explorative approach adopted in our investigation, it is interesting to note how well the function  $\chi$  captures the main properties of the instability growth time and how it identifies the model with the strongest instability along a sequence. This provides interesting pointers towards future work. First of all, one should investigate if our empirical expression remains useful also for other models, eg. different polytropic indices and rotational laws. If the suggestion proves robust one should also try to understand the underlying physics. This might shed useful light on the nature of this class of instabilities.

Before moving on, let us point out that most of the numerical results have been presented in dimensionless units, and the shortest growth time calculated in this work is  $\tau = 29.25/\sqrt{G\rho_m}$  for a model with  $A = 0.4$  and axis ratio  $R_p/R_{eq} = 0.4$ . In physical units, this value is  $\tau = 5.13$  ms, for a typical star with  $M = 1.4M_\odot$  and EoS parameters  $\gamma = 2$  and  $k = 6.674 \cdot 10^4 \text{ g}^{-1} \text{ cm}^5 \text{ s}^{-2}$ .

#### 4 A SLIGHT ASIDE: THE INERTIAL R-MODES

The perturbative time-evolution code obviously allows us to consider a wider range of problems involving differentially rotating stars. As a pertinent example, let us make some comments on the inertial r-modes. These modes are rotationally restored by the Coriolis force and are of particular interest since they suffer the gravitational-wave instability already at low rotation rates in uniform stars. Much effort has gone into understanding the astrophysical relevance of this instability, eg. the role of various internal viscosity mechanisms, but the bulk of the work has considered stars in uniform rotation. If the r-mode instability acts very early

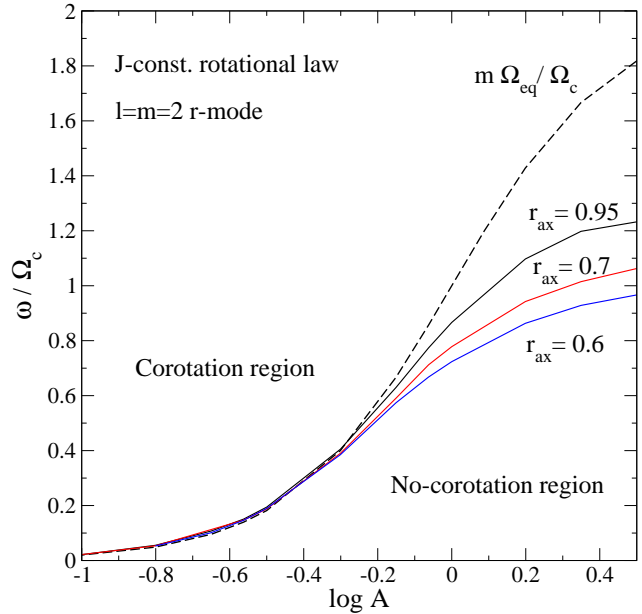


**Figure 8.** This figure shows the dependence of the  $l = m = 2$  r-mode on the differential rotation parameter  $A$ , for three stellar configurations with a fixed axis ratio. They are, respectively,  $r_{ax} = 0.95, 0.7$  and  $0.6$  (see legend). The dashed line denotes the equatorial boundary of the co-rotation region. The horizontal axis displays the quantity  $\log A$  while the vertical axis gives the ratio between the mode frequency and the central angular velocity of the star. This figure can be directly compared to Fig. 4 of Karino et al. (2001), where the numerical method became unreliable as the mode approached the co-rotation region.

on in a neutron star’s life or is triggered in the hot remnant immediately after binary neutron star merger, then we would need to understand how differential rotation affects the mechanism. It is easy to see that the co-rotation point could be relevant for this discussion. According to an inertial observer the r-mode is prograde for any stellar rotation rate with a frequency proportional to the bulk rotation rate (like all inertial modes). If such a mode enters the co-rotation region it should do so by crossing the low-frequency boundary which corresponds to the equatorial angular velocity  $\Omega_{eq}$  (at least for “reasonable” rotation laws like the j-constant law).

However, it is not clear from the results in the literature if the r-mode actually enters the co-rotation region. So far, the r-mode frequency in differentially rotating stars has only been determined in Newtonian gravity by Karino et al. (2001). For a  $\gamma = 2$  polytrope and the j-constant rotation law, their results show that the r-mode is not in co-rotation for stars with  $A > 0.6$ . However, the mode clearly approaches the co-rotation band when  $A \rightarrow 0.6$ . Unfortunately, the numerical code used by Karino et al. (2001) was not accurate for higher degrees of differential rotation (presumably because the co-rotation point corresponds to a singularity in the frequency domain description of the problem). As our numerical framework is based on time evolving the perturbation equations, our analysis is not affected by this issue and we can determine the r-mode frequency for lower values of  $A$ . This allows us to check if the r-mode goes in co-rotation for a high degree of differential rotation. To carry out this exercise, we use the Cowling approximation which

is known to provide accurate results for the r-mode frequency (Karino 2003). Considering models with a fixed axis ratio,  $r_{ax} = R_p/R_{eq}$ , respectively,  $r_{ax} = 0.95, 0.7$  and  $0.6$ , we determine the  $l = m = 2$  r-mode frequency for  $A = 0.1 - 10$ . The results are shown in Figure 8. We find that, even though the r-mode approaches the co-rotation region as the degree of differential rotation is increased, it never really enters the co-rotation region (more than marginally). In all cases we have considered, the r-mode stays very close to the equatorial boundary, i.e.  $\omega \simeq m\Omega_{eq}$ , as the rotation rate increases. We have found no evidence that the r-mode suffers a shearing instability analogous to the low  $T/W$  instability in the f-mode. It is not clear whether this is because no such instability exists or if it is simply the case that the growth time is too large to overcome the numerical dissipation in the examples we have studied (as one would expect for a mode located at the boundary of the co-rotation region).

## 5 CONCLUDING REMARKS

We have developed a framework for numerical time evolutions of linear perturbations of differentially rotating, Newtonian, stars. Within this framework we have carried out a large parameter survey for polytropic stars described by the standard j-constant rotation law, focussing on the fundamental f-mode and the low  $T/W$  instability. Our results for the instability growth time confirm the assertion of Watts et al. (2005) that the instability sets in at the point when the f-mode first enters the co-rotation region (when there is a point in the star where the pattern speed in the star matches the local rotation rate of the background fluid). We have used the integrands of the canonical energy and angular momentum to highlight the close relationship between the instability and the co-rotation point. By considering the relevant stellar parameters we have also obtained a relatively simple empirical relation which describes how the growth rate of the low  $T/W$  instability increases as the f-mode moves into the co-rotation region, reaches a maximum and then tapers off as the mode exits the unstable region again.

Our analysis has, in many ways, been of an exploratory nature. Our main aim was to map out the relevant parameter space and provide clear evidence for the link between the co-rotation boundary and the onset of instability. As they stand the results seem convincing in this respect. This is quite an important conclusion because it would be sufficient to know that the f-mode of a given configuration lies inside the co-rotation region to know that the mode should be (at least in principle) unstable. Further work is needed to confirm this conclusion for other rotation laws and more realistic equations of state, but we have no reason to expect that the qualitative behaviour would change much in other cases. More detailed work is also needed in order to explain the form of the empirical relation we have found for the instability growth rate. Ideally, one would like to be able to derive this result from underlying principles, but this seems like a very difficult problem. One might be able to make progress using the canonical energy/angular momentum arguments from Friedman & Schutz (1975, 1978a,b). However, this would likely require a frequency domain approach which would be hampered by the singularity associated with the

co-rotation point. Unfortunately, the fact that the instability analysis only holds (strictly) for inviscid systems means that we have been unable to use our results to make progress in this direction (the numerical simulations involve the standard artificial viscosity to stabilize the evolutions). We have also not been able to extract the mode eigenfunctions with sufficient precision due to the exponential growth of the perturbation variables during the instability. It seems possible that future work could do better in this regard. We would certainly encourage efforts in this direction.

Finally, we used our computational framework to consider the inertial r-modes. In this case, our results extend previous work to higher degrees of differential rotation. We have demonstrated that the r-modes do not (at least for our stellar models) evolve into the co-rotation region. Rather, they remain near the boundary of this region for rapidly and differentially rotating stars. This is an interesting result in its own right, and a clear demonstration of the usefulness of our numerical framework. The result may also be relevant for relativistic studies of the r-mode where the frame-dragging provides an effect that is qualitatively similar to differential rotation. For non-barotropic stars, in particular, the relativistic r-mode problem is known to be complicated. Based on the present evidence it would be tempting to suggest that time-evolutions of the kind used in the present work may prove a powerful tool also in that setting.

## ACKNOWLEDGEMENTS

AP acknowledges support from the European Union Seventh Framework Programme (FP7/2007-2013) under grant agreement no. 267251 “Astronomy Fellowships in Italy (AstroFit)”. NA acknowledges support from STFC in the UK and generous hospitality from the Institute for Nuclear Theory at the University of Washington where some of this work was carried out.

## REFERENCES

- Andersson N., 2003, *Class. and Quantum Grav.*, 20, 105
- Baiotti L., Pietri R. D., Manca G. M., Rezzolla L., 2007, *Phys. Rev. D*, 75, 044023
- Camarda K. D., Anninos P., Fragile P. C., Font J. A., 2009, *ApJ*, 707, 1610
- Centrella J. M., New K. C. B., Lowe L. L., Brown J. D., 2001, *ApJ*, 550, L193
- Cerdá-Durán P., Quilis V., Font J. A., 2007, *Computer Physics Communications*, 177, 288
- Chandrasekhar S., 1969, *Ellipsoidal figures of equilibrium* (New Haven, CT: Yale University Press)
- Chandrasekhar S., 1970, *Phys. Rev. Lett.*, 24, 611
- Corvino G., Rezzolla L., Bernuzzi S., De Pietri R., Giacomazzo B., 2010, *Class. and Quantum Grav.*, 27, 114104
- Franci L., De Pietri R., Dionysopoulou K., Rezzolla L., 2013, *Phys. Rev. D*, 88, 104028
- Friedman J. L., Schutz B. F., 1975, *ApJ*, 200, 204
- Friedman J. L., Schutz B. F., 1978a, *ApJ*, 221, 937
- Friedman J. L., Schutz B. F., 1978b, *ApJ*, 222, 281
- Fu W., Lai D., 2011, *MNRAS*, 413, 2207
- Hachisu I., 1986, *ApJSS*, 61, 479

- Jones D. I., Andersson N., Stergioulas N., 2002, MNRAS, 334, 933
- Karino S., 2003, MNRAS, 343, 175
- Karino S., Yoshida S., Eriguchi Y., 2001, Phys. Rev. D, 64, 024003
- Karino S., Yoshida S., Eriguchi Y., 2001, Phys. Rev. D, 64, 024003
- Kuroda T., Umeda H., 2010, ApJS, 191, 439
- Muhlberger C. D., Nouri F. H., Duez M. D., Foucart F., Kidder L. E., Ott C. D., Scheel M. A., Szilágyi B., Teukolsky S. A., 2014, arXiv:1405.2144
- Ott C. D., Dimmelmeyer H., Marek A., Janka H.-T., Hawke I., Zink B., Schnetter E., 2007, Phys. Rev. Lett., 98, 261101
- Ott C. D., Ou S., Tohline J. E., Burrows A., 2005, ApJ, 625, L119
- Ou S., Tohline J. E., 2006, ApJ, 651, 1068
- Papaloizou J. C., Pringle J. E., 1980, MNRAS, 190, 43
- Papaloizou J. C. B., Pringle J. E., 1984, MNRAS, 208, 721
- Passamonti A., Haskell B., Andersson N., Jones D. I., Hawke I., 2009a, MNRAS, 394, 730
- Passamonti A., Haskell B., Andersson N., 2009b, MNRAS, 396, 951
- Saijo M., Baumgarte T. W., Shapiro S. L., 2003, ApJ, 595, 352
- Saijo M., Yoshida S., 2006, MNRAS, 368, 1429
- Scheidegger S., Fischer T., Whitehouse S. C., Liebendörfer M., 2008, A&A, 490, 231
- Schutz B. F., 1980a, MNRAS, 190, 21
- Schutz B. F., 1980b, MNRAS, 190, 7
- Shibata M., Baumgarte T. W., Shapiro S. L., 2000, ApJ, 542, 453
- Shibata M., Karino S., Eriguchi Y., 2002, MNRAS, 334, L27
- Shibata M., Karino S., Eriguchi Y., 2003, MNRAS, 343, 619
- Watts A. L., Andersson N., Jones D. I., 2005, ApJ, 618, L37